

## WAVE-INDUCED FORCES ON THE GIANT KELP *MACROCYSTIS PYRIFERA* (AGARDH): FIELD TEST OF A COMPUTATIONAL MODEL

BARBARA D. UTTER AND MARK W. DENNY\*

Department of Biological Sciences, Stanford University, Hopkins Marine Station, Pacific Grove, CA 93950, USA

Accepted 30 August 1996

### Summary

We propose a hydro-mechanical numerical model that predicts the maximal tension to which stipes of the giant kelp *Macrocystis pyrifera* will be subjected when exposed to ocean waves. Predicted maximal tensions are close to those measured in the field. The strength of *Macrocystis pyrifera* stipes was measured, allowing our prediction of forces to be translated into a prediction of the fraction of stipes broken. Predicted breakage is low even for extreme storm waves, a testament to the mechanical design of individual kelp fronds. However, empirically measured rates of kelp

mortality can be high, considerably higher than those predicted on the basis of hydrodynamic forces acting alone. This indicates that factors not taken into account in our model (such as holdfast dislodgment, entanglement of stipes, damage from herbivory and wave breaking) contribute substantially to mortality in *Macrocystis pyrifera*.

Key words: algal mechanics, kelp, linear wave theory, *Macrocystis pyrifera*, subtidal ecology, wave exposure, wave forces.

### Introduction

The velocities and accelerations accompanying ocean waves can impose large hydrodynamic forces on marine organisms, including kelps (e.g. Denny, 1988; Seymour *et al.* 1989; Vogel, 1994; Friedland and Denny, 1995). A variety of mechanical strategies have been proposed by which organisms cope with these forces (Koehl, 1984, 1986; Denny, 1988; Johnson and Koehl, 1994; Friedland and Denny, 1995). Of particular importance are strategies pertaining to very large kelps. For example, Koehl and Wainwright (1977) suggest that the bull kelp *Nereocystis luetkeana* avoids the brunt of hydrodynamic forces by 'going with the flow', a strategy facilitated by this species' flexibility and great length, and by the extensibility of its stipe material. *Macrocystis pyrifera*, the giant kelp, is similar in size and flexibility to *N. luetkeana* and has similar materials properties; it may thus employ a similar strategy. This strategy gives no guarantee, however, that these plants will not be broken. Indeed, wave forces imposed during storms tear both *N. luetkeana* and *M. pyrifera* stipes from the rest of the plant and even dislodge entire holdfasts (Koehl and Wainwright, 1977; Seymour *et al.* 1989).

Despite the recognition of wave-induced hydrodynamic forces as a source of mortality in the giant kelp, the mechanics of the interaction between *M. pyrifera* and moving water have received little attention. Jackson and Winant (1983) calculated the drag on *M. pyrifera* fronds, but modeled the fronds as rigid, vertical pillars in a horizontal flow. This approximation was sufficient for their purpose (which was to estimate the damping effect of kelp on currents), but is clearly an oversimplification

of the dynamics of this flexible structure. Seymour *et al.* (1989) explored various aspects of wave-induced water motion that can potentially affect the mortality of kelps and showed how maximal predicted water velocity is well correlated with kelp dislodgment. However, their work did not extend beyond a qualitative description of the mechanics of kelps in wave-induced flows. Direct measurements of forces on *M. pyrifera* are virtually absent. In the sole report found in the literature, Neushul *et al.* (1967) measured a force of 90 N on a *M. pyrifera* plant of 38 fronds, but the water motion leading to this force was described only as a 'moderate surge'.

Here, we explore the dynamics of wave-exposed kelps through the use of a hydro-mechanical numerical model that predicts the forces imposed by waves of a given height and period. These predictions are tested against short-term measurements made in the field and are used as the basis for a preliminary examination of the role of wave-induced forces in the long-term survivorship of *M. pyrifera*.

### Materials and methods

#### Macrocystis pyrifera

An individual *Macrocystis pyrifera* (Agardh) plant consists of a conical holdfast from which several rope-like stipes emerge (Fig. 1). These basal stipes branch dichotomously a short distance above the holdfast to form numerous distal stipes that extend without further branching. Elongated, irregularly corrugated blades branch off one side of each stipe at intervals, the distance

\*Author for correspondence (e-mail: mwdenny@leland.stanford.edu).

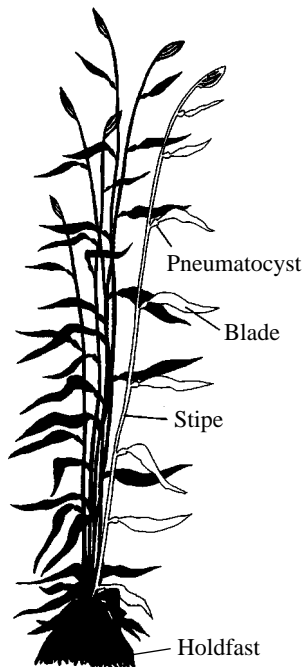


Fig. 1. *Macrocystis pyrifera*.

between blades being greatest near the holdfast. The blades increase in area from the holdfast towards the free end of the stipe to a point half to two-thirds of the way along the stipe and then decrease in area distally (North, 1971). A small gas bladder, the pneumatocyst, is present at the base of each blade. The combination of a stipe and its attached pneumatocysts and blades is referred to here as a frond. Stipes may reach a length of 45 m, and plants typically grow at depths of 7–20 m (North, 1971).

#### A numerical model of kelp mechanics

##### The water column

A model of the nearshore water column is shown in Fig. 2. Water of depth  $d$  overlies a horizontal seafloor, and all motions of both the water and the kelp are assumed to occur in a vertical plane parallel to the direction of wave propagation. Position in the vertical plane is described using a Cartesian coordinate system with its origin at the seafloor. The  $x$ -axis extends horizontally with values increasing in the direction of wave propagation, and the  $y$ -axis is vertical with positive values above the seafloor.

An individual kelp frond is modeled by a point element tethered to the substratum by a flexible, extensible stipe (Fig. 2). The point element has a mass,  $M$ , equal to that of the entire frond and is subject to the same forces as the entire kelp frond. The stipe is assumed to have a tensile stiffness when stretched beyond its resting length, but no compressive or bending stiffness, and is firmly attached to the seafloor at  $(x=0, y=0)$ .

At any instant, the point element is located at position  $(x, y)$  and has a velocity  $\mathbf{u}_k$  and an acceleration  $\mathbf{a}_k$ . The instantaneous velocity of the water relative to the seafloor is  $\mathbf{u}_w$  and its acceleration is  $\mathbf{a}_w$ . The velocity of the water relative to the

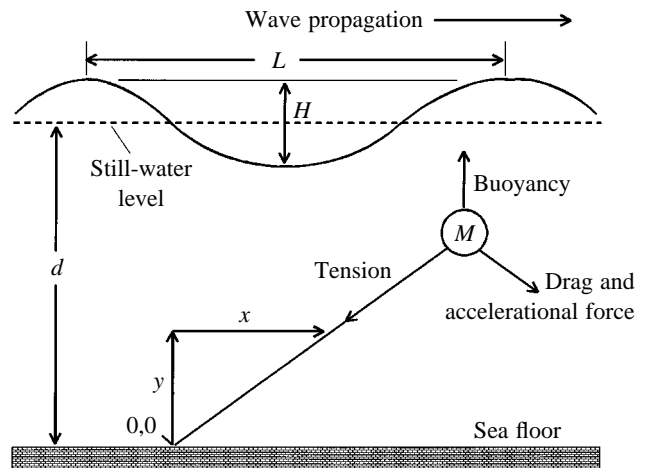


Fig. 2. A schematic representation of the components of the numerical model of kelp mechanics.  $d$ , water depth;  $x, y$ , horizontal and vertical components of kelp position in the vertical plane;  $M$ , mass of point element representing kelp frond;  $H$ , wave height;  $L$ , wavelength. Not drawn to scale.

point element is  $\mathbf{u}_r = \mathbf{u}_w - \mathbf{u}_k$  and the acceleration of the water relative to the element is  $\mathbf{a}_r = d\mathbf{u}_r/dt$ , where  $t$  is time. Note that all variables shown in bold type are vectors.

##### Hydrodynamic forces

The point element moves in response to the forces placed upon it: buoyancy, drag, the accelerational force and the tension exerted by the stipe (Koehl and Wainwright, 1977; Koehl, 1986; Denny 1987, 1988; Carrington, 1990; Bell, 1992; Gaylord *et al.* 1994; Friedland and Denny, 1995). Although lift can be substantial for benthic animals (Denny, 1987, 1988, 1989; Denny *et al.* 1985), the lift that a giant kelp experiences is likely to be inconsequential in comparison with the accelerational force or drag (Denny, 1988; Gaylord *et al.* 1994) and, on this basis, it is not included in the present analysis.

**Buoyancy.** Because the frond has a different density from that of its fluid surroundings, it is subject to a net buoyant force:

$$\mathbf{B} = -gV(\rho_k - \rho_w), \quad (1)$$

where  $g$  is the gravitational acceleration,  $V$  is the volume of fluid displaced by the frond,  $\rho_w$  is the density of sea water (approximately  $1025 \text{ kg m}^{-3}$ ) and  $\rho_k$  is the overall density of the frond. A positive value of  $\mathbf{B}$  denotes a force acting vertically upwards. *M. pyrifera* fronds are positively buoyant owing to their pneumatocysts.

**Drag.** As a fluid flows past the frond, drag,  $\mathbf{F}_d$ , is imposed in the direction of flow. This force can be modeled by the relationship (Gaylord *et al.* 1994; Denny, 1995):

$$\mathbf{F}_d = (1/2)\rho_w \mathbf{u}_r^\beta A S_d. \quad (2)$$

$\beta$  (the velocity exponent) is approximately 2 for bluff objects at high Reynolds numbers, but is likely to be less than 2 for streamlined objects such as kelp fronds (Vogel, 1984, 1994; Gaylord *et al.* 1994).  $A$  is the maximal projected area of the frond (approximately half its wetted area) and  $S_d$  is an empirically determined shape coefficient.

**Accelerational force.** When a kelp frond accelerates in an accelerating fluid (as is often the case), an accelerational force,  $\mathbf{F}_a$ , is imposed which is a combination of two forces (Denny *et al.* 1985; Koehl, 1986; Denny, 1988; Gaylord *et al.* 1994). First, there is a mass of fluid (the added mass) that acts as if it is accelerated with the frond (Denny, 1988; Gaylord *et al.* 1994). The force required to accelerate this added mass is  $\rho_w C_a V \mathbf{a}_r$  where  $C_a$  is the dimensionless added mass coefficient and  $V$  is again the volume of fluid displaced by the object. Second, there is  $\rho_w V \mathbf{a}_w$ , the force imposed by the pressure gradient associated with the acceleration of the fluid relative to the seafloor (Batchelor, 1967).

Thus, the accelerational force  $\mathbf{F}_a$  is:

$$\mathbf{F}_a = \rho_w C_a V \mathbf{a}_r + \rho_w V \mathbf{a}_w. \quad (3)$$

#### Water motion

From equations 2 and 3, it is apparent that the external force imposed on a kelp is governed in large part by the motion of water, which for ocean waves can be described by linear wave theory (Kinsman, 1965; Denny, 1988). The horizontal wave-induced velocity,  $u$ , of the fluid at position  $(x, y)$  is:

$$u = \frac{\pi H}{T} \cos(kx - \omega t) \frac{\cosh(ky)}{\sinh(kd)}, \quad (4)$$

where  $H$  is the wave height (the vertical distance between trough and crest, see Fig. 2) and  $T$  is the wave period. Note that  $d$ , the water's depth, is measured from the still-water level rather than the instantaneous surface elevation in the wave. The wave number,  $k$ , is:

$$k = 2\pi/L, \quad (5)$$

where  $L$  is the wavelength at depth  $d$  (Eckart, 1952):

$$L \cong \frac{gT^2}{2\pi} \sqrt{\tanh(4\pi^2 d/T^2 g)}. \quad (6)$$

The radian wave frequency,  $\omega$ , is:

$$\omega = 2\pi/T. \quad (7)$$

The vertical water velocity,  $v$ , is:

$$v = \frac{\pi H}{T} \sin(kx - \omega t) \frac{\sinh(ky)}{\sinh(kd)}, \quad (8)$$

and the overall water velocity,  $\mathbf{u}_w$ , is the vector sum of  $u$  and  $v$ :

$$\mathbf{u}_w = \sqrt{u^2 + v^2}, \quad (9)$$

with direction  $\arctan(v/u)$  relative to the  $x$ -axis. The horizontal,  $a_x$ , and vertical,  $a_y$ , accelerations are:

$$a_x = \frac{2\pi^2 H}{T^2} \sin(kx - \omega t) \frac{\cosh(ky)}{\sinh(kd)}, \quad (10)$$

$$a_y = -\frac{2\pi^2 H}{T^2} \cos(kx - \omega t) \frac{\sinh(ky)}{\sinh(kd)}, \quad (11)$$

and the overall acceleration is:

$$\mathbf{a}_w = \sqrt{a_x^2 + a_y^2}, \quad (12)$$

with direction  $\arctan(a_y/a_x)$  relative to the  $x$ -axis.

As waves arrive at the shore from different sources, their amplitudes combine, resulting in a distribution of heights known as the Rayleigh distribution (Longuet-Higgins, 1952, 1980; Denny, 1995). The maximal wave height,  $H_m$ , of a set of Rayleigh-distributed waves can be expressed as a function of time,  $t$ :

$$H_m = 0.6541 \{ \sqrt{\ln(t+T)} + 0.2886 [1/\sqrt{\ln(t/T)}] \} H_s, \quad (13)$$

where the significant wave height,  $H_s$ , is the average height of the highest one-third of waves present at a site during the period in question (Longuet-Higgins, 1952, 1980; Denny, 1993, 1995).  $H_s$  is usually estimated as  $4(m_0)^{1/2}$ , where  $m_0$  is the variance of the sea surface elevation (Longuet-Higgins, 1980). Given  $H_s$  and  $T$ , the maximal wave height expected in a given period  $t$  can be predicted and used to calculate the maximal velocities and accelerations present beneath the wave (Denny, 1995).

#### Tension

Tension in the stipe is a function of stipe cross-sectional area and of how far the stipe is stretched. For a stipe of unstretched length  $l_0$  and cross-sectional area  $A_{xs}$ :

$$\mathbf{F}_t = 1.91 \times 10^7 \left( \frac{\sqrt{x^2 + y^2} - l_0}{l_0} \right)^{1.4068} A_{xs} \quad \text{for } \sqrt{x^2 + y^2} > l_0 \quad (14)$$

$$\mathbf{F}_t = 0 \quad \text{for } \sqrt{x^2 + y^2} \leq l_0,$$

where  $(x, y)$  is the location of the point element at the end of the stipe. The force of tension,  $\mathbf{F}_t$ , is measured in newtons and the cross-sectional area,  $A_{xs}$ , is measured in square meters. This expression is derived from a typical stress-strain curve for *M. pyrifera* (Fig. 3). The tension in an extended stipe is directed along the stipe; that is, at an angle  $\arctan(y/x)$  to the horizontal. We assume that the stipe is elastic; that is, no energy is lost to viscosity as the stipe is stretched. This is a reasonable assumption in that stipes of *M. pyrifera* appear to be similar in their mechanical properties to those of *N. luetkeana*, and *N. luetkeana* stipes are elastic, at least for small extensions (Johnson and Koehl, 1994).

#### Force balance

The instantaneous change in velocity of the point element is calculated from the force balance for the element-stipe system:

$$M_e \mathbf{a}_k = \mathbf{B} + \mathbf{F}_d + \mathbf{F}_a + \mathbf{F}_t, \quad (15)$$

where  $M_e$  is the total effective mass of the frond,

$$M_e = M + \rho_w C_a V, \quad (16)$$

and  $M$  is the mass of the frond. Thus:

$$\mathbf{a}_k = \frac{\mathbf{B} + \mathbf{F}_d + \mathbf{F}_a + \mathbf{F}_t}{M_e}, \quad (17)$$

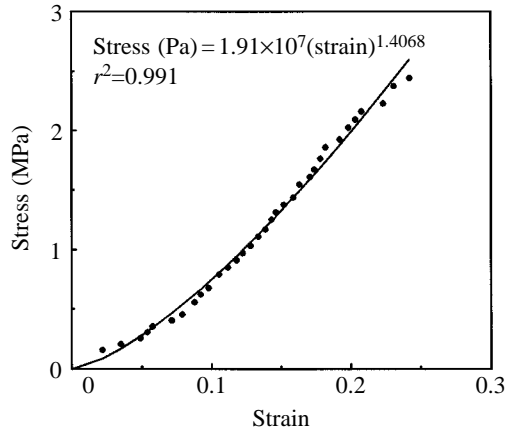


Fig. 3. The stress–strain curve for an *M. pyrifera* stipe used as a basis for computation in the numerical model. Unpublished data from W. Hoese.

Equation 17 is numerically integrated through time to give  $u_k$  and  $(x,y)$ .

To tailor this simple model to the dimensions of an actual kelp frond, we locate the point element at the center of drag of the frond, thus setting the effective length of the stipe. This effective length,  $l_0$ , is calculated as:

$$l_0 = \frac{\sum_{i=1}^N (1/2)l_i \rho_w u_{i,max}^\beta A_i S_d}{\sum_{i=1}^N (1/2)\rho_w u_{i,max}^\beta A_i S_d}, \quad (18)$$

where  $l_i$  is the distance from the seabed to the midpoint of the  $i$ th length segment on the frond (here taken in 1 m increments),  $A_i$  is the maximal projected area for that specific segment and  $u_{i,max}$  is the maximal horizontal velocity at that depth (equation 4).  $N$  is the total number of segments in the plant.

If, in the course of the calculations, the point mass-force element of the model frond is projected to move above the

surface of the water in the next increment of time, its position is adjusted to lie at the surface and its vertical velocity is set equal to that of the surface. The model does not attempt to incorporate any effects of wave breaking.

*Experimental measurements*

*Drag*

*M. pyrifera* fronds, cut near the holdfast, were collected on three separate occasions in August 1989 from Cabrillo Point, California (36°37' N, 121°54' W), adjacent to Hopkins Marine Station. The fronds were numbered and placed in an outdoor tank with a continuous flow of sea water. Measurements were made on the fronds within 48 h of collection.

Drag was measured on six fronds using the apparatus shown in Fig. 4. A triangular wooden plate (1.25 m base, 1.8 m high, 2 cm thick) was held vertically in the water by a frame clamped to the gunwales of a boat, providing a stable base from which drag and velocity could be measured. A spring scale was mounted on the frame. A string ran from the end of the spring scale over a pulley fastened to the frame above the triangular plate and down through a hollow fairing in the trailing edge of the plate. The string then ran through a second pulley attached to the lowest point of the triangular plate and extended 8 m behind the boat, where it was tied to a piece of stiff aluminum wire. The base of a *M. pyrifera* frond was lashed to the aluminum wire using 3 mm diameter rubber tubing. A Marsh-McBirney model 511 electromagnetic flow meter with its probe attached to the wooden plate measured the speed of the plate (and the frond) through the water.

Each frond was subjected to velocities between 0.6 and 3 m s<sup>-1</sup>. While the boat was driven at a constant velocity, one person called out the instantaneous force measured by the spring scale and another read the corresponding velocity and recorded both measurements. Seven to fifteen readings were taken at each velocity, and four to seven different velocities were used for each run. Four runs constituted one trial; one trial was conducted on each frond.

After each trial, the frond was traced onto paper. The trace was cut out, weighed and compared with the weight of a known

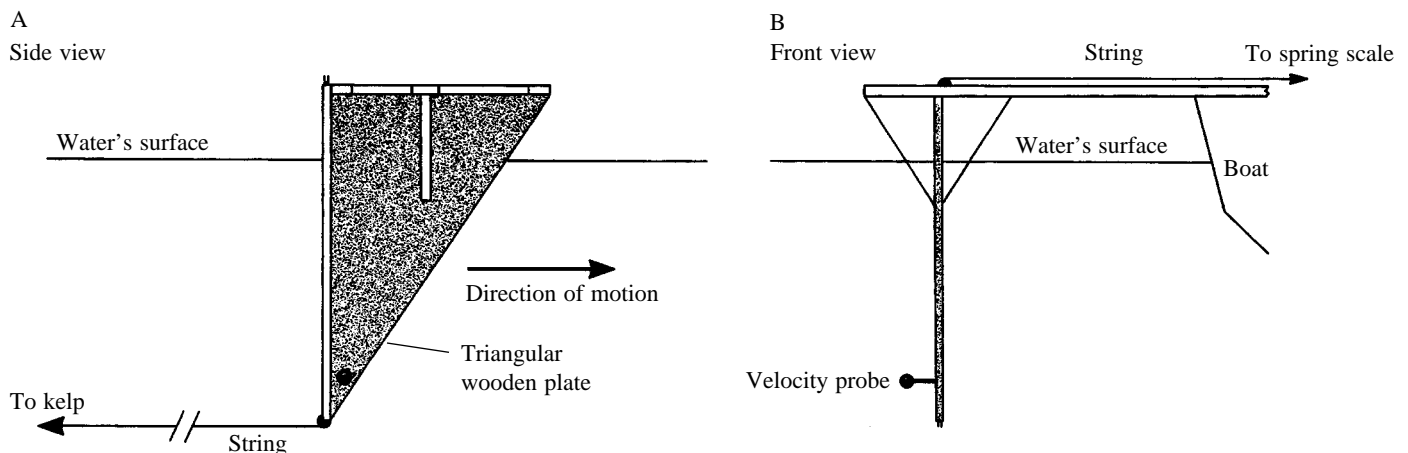


Fig. 4. An apparatus for measuring the drag on *M. pyrifera*. (A) Side view; (B) front view. See text for further details.

area of paper to provide an estimate of maximal projected area,  $A$ .

The shape coefficient,  $S_d$ , and velocity exponent,  $\beta$ , in equation 2 were calculated using the combined data from the six fronds by regressing the records of drag force [per  $(1/2)\rho_w A$ ] against velocity using untransformed data and a simplex algorithm with a least-squares criterion for the goodness of fit (Caceci and Cacheris, 1984).

#### Tensile tests

Individual stipes were tested in August 1991 to determine their breaking stress. Fronds were collected and stored as described previously. Twenty-five tensile tests were performed, each on a stipe section between two adjacent blades. The upper end of each section was lashed to a horizontal wooden dowel and suspended from the ceiling. The other end was tied in a similar fashion to a lower dowel from which a bucket was hung. Force was then applied to each stipe by slowly adding water to the bucket. When the stipe broke, the water was turned off and the bucket and water were weighed to the nearest 0.057 kg. A negligible amount of water entered the bucket after the stipe broke and before the water was turned off. Nominal breaking stress was expressed as the weight applied to the stipe at breaking divided by the initial cross-sectional area of the stipe.

The variation in measured breaking stress among samples provides a means to estimate the probability that a *M. pyrifera* stipe chosen at random has a strength less than a given value. The stresses needed to break the stipes were ranked in ascending order. The probability,  $P(\sigma_i)$ , of having a breaking stress,  $\sigma_i$ , less than that of a stipe with rank  $i$  is:

$$P(\sigma_i) = i/(N + 1), \quad (19)$$

where  $N$  is the total number of stipes tested, in this case 25 (Gumbel, 1958). These estimates of the cumulative probability of breaking stress were fitted to a Weibull (lower bound) equation (Sarpkaya and Isaacson, 1981):

$$P(\sigma) = 1 - \exp \left[ - \left( \frac{\sigma - a}{b} \right)^c \right]. \quad (20)$$

The best-fit coefficients  $a$ ,  $b$  and  $c$  were determined using a simplex algorithm and a least-squares criterion for the goodness of fit (Caceci and Cacheris, 1984).

#### Field measurements

Measurements of maximum wave-induced forces were obtained in the field for 10 individual *M. pyrifera* fronds. For each trial, maximal force on a frond was recorded by two spring scales (Bell and Denny, 1994). The spring of one scale was relatively compliant and measured small forces (1–12 N); the second was stiffer and was able to measure forces from 10 to 60 N. The scales were attached in series with 30 lb (13.5 kg) test nylon monofilament fishing line (the total length of the apparatus was approximately 40 cm) and placed between two small wooden dowels (3 mm diameter). Each stipe was cut *in situ*, and a dual-spring scale was inserted between the ends and

lashed to the stipe using rubber tubing. Maximum force measurements were monitored by an observer using SCUBA, and the scales were reset after each reading. Spring scales were calibrated before and after field use by hanging known weights from the scales.

The study was conducted between 5 May and 5 June 1992 at Point Joe (36°35' N, 121°57' W), a fully wave-exposed site off of Pebble Beach, California. On each occasion, transducers were inserted into stipes at depths ranging from 14.2 to 14.8 m. Each spring scale was checked 2 and 7 days after installation. For seven of the stipes, two successful trials were conducted; for the three other stipes, a single trial was conducted. After completion of the trials, the experimental stipes were removed and the stipe cross-sectional area and frond area were noted for every meter along the stipe. The stipe cross-sectional area was estimated by measuring the maximal and minimal diameter of a cross section and calculating the area as for an ellipse. Frond area was obtained from paper tracings of the frond as described above. The mass of each frond was estimated from a previously determined relationship between mass and maximal projected area. For fronds of length 11–20 m, there was no significant correlation between length and  $M/A$ . The average ratio of  $M$  (in kg) to  $A$  (in  $m^2$ ) is  $0.774 \pm 0.04$  (S.E.M.,  $N=8$ ).

Force due to buoyancy was measured for each frond by hanging brass weights (their weight corrected for buoyancy in sea water) from individual fronds in a tank of sea water until the fronds were neutrally buoyant.

Significant wave heights and the wave period at peak spectral density were obtained for the experimental periods using a bottom-mounted recording pressure transducer installed at the Point Joe site by the Monterey Bay Aquarium. The pressure records thus obtained were corrected for the depth of the transducer (Denny, 1988). For use in the model, we noted the maximal significant wave height present during the period when fronds were instrumented and assumed that this  $H_s$  was constant for 8 h, the full time between measurements of  $H_s$ .

#### Model implementation

Equation 17 was solved simultaneously for its  $x$  and  $y$  components using a fourth-order Runge–Kutta algorithm (Dahlquist and Björk, 1974) and a time step of 0.001 s. Variables were initialized at  $t=0$  such that  $x=v=0$ , and the vertical position of the point element  $y$  was equal to the effective stipe length induced by buoyancy. Tension was calculated for three wave periods and the maximum tension was recorded in each period.

To explore the potential effect of the initial conditions on the maximal tension, two initial conditions were chosen. In the first, the initial horizontal velocity of the point element was set to 0. In the second, the initial horizontal velocity was set equal to that of the surrounding water,  $\pi H/T$ .

Gaylord *et al.* (1994) measured the added mass coefficient for three species of macroalgae and found values ranging from 1.6 to 6.7, with an average of about 4. Unfortunately, the algae tested by Gaylord *et al.* (1994) are all much smaller than *M.*

*pyrifera* and it is uncertain where in this range the  $C_a$  for *M. pyrifera* might fall. To explore the effect of the added mass on the maximum tension, the added mass coefficient was varied from 1 to 4. Values in excess of 4 led to results that were clearly at odds with reality.

## Results

### Drag data

Results of the drag experiments are shown in Fig. 5. The best-fit shape coefficient,  $S_d$ , is 0.0148 and  $\beta$  is 1.596. Similar results have been seen in other macroalgae and vascular plant leaves (Vogel, 1984, 1989; Carrington, 1990; Gaylord *et al.* 1994). The scatter in the results shown in Fig. 5 is probably due to the continual reorientation of the fronds as they were towed and is typical of macroalgae in flow (see Carrington, 1990; Bell, 1992).

### Tensile tests

The probability that a *M. pyrifera* frond chosen at random has less than a given breaking stress,  $\sigma$  (in Pa), is described by the equation:

$$P(\sigma) = 1 - \exp \left[ - \left( \frac{\sigma - 1.00}{3.16 \times 10^6} \right)^{3.75} \right]. \quad (21)$$

This expression is plotted in Fig. 6. A regression of values predicted by equation 21 against the actual data shows that this relationship accounts for 99.0% of the measured variation in probability of breakage.

### Field data

During the experimental period, Point Joe was relatively calm – significant wave heights varied from 0.85 to 2.71 m. In the 17 trials, fronds encountered maximal forces of 1.4–30.9 N (Table 1). The stresses caused by these tensions (0.04–0.68 MPa) are small compared with the breaking strength of *M. pyrifera* stipes ( $2.82 \pm 0.172$  MPa, mean  $\pm$  S.E.M., Fig. 6).

### Model data

The results from our model were compared with the 17 field trials by computing the fractional error,

$$\text{fractional error} = \frac{\text{predicted tension} - \text{measured tension}}{\text{predicted tension}}, \quad (22)$$

and averaging over all trials.

The best fit of the model to the field data (as determined by the lowest fractional error averaged across wave cycles) was obtained with an added mass coefficient of 3 (Table 2). An added mass coefficient of 4 yielded mean fractional errors of similar magnitude, but with substantially larger standard errors. The best-fit added mass coefficient of 3 is smaller than the average of 4 measured by Gaylord *et al.* (1994), but this is perhaps not surprising given the fact that *M. pyrifera* fronds are more streamlined (have a lower  $S_d$ ) than those of the three

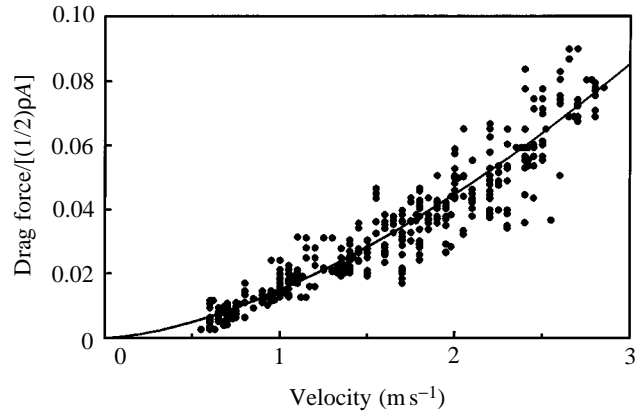


Fig. 5. Drag force per  $(1/2)\rho_w A$ , where  $\rho_w$  is the density of sea water and  $A$  is the maximal projected area of the frond, as a function of water velocity for *M. pyrifera*. The data shown are 476 randomly sampled points from a set of 1536 points, and the solid line is the best-fit regression to the entire data set.

species examined by Gaylord *et al.* (1994). Subsequent predictions of our model were made with  $C_a=3$ . The predicted tensions vary slightly among the three wave cycles for which the model was computed (Table 1). Variation in maximum force from one cycle to the next could be due to the slow evolution of the system towards a repeatable response to the forcing function or to an inherent property of this flexible mechanical system, attributable at least in part to nonlinearities such as the discontinuity in the stiffness of the stipe at its unstretched length. A small physical model of a similar system (a sphere with slight positive buoyancy tethered by an elastic string) has been shown to exhibit chaotic dynamics (M. W. Denny, unpublished data).

Force predictions from our numerical model were close to the forces observed in the field (Table 1). The average fractional error of the predictions is 0.24–0.30 depending on the cycle. In other words, on average, the model overestimates the force imposed on fronds in the field by 24–30% of the predicted force.

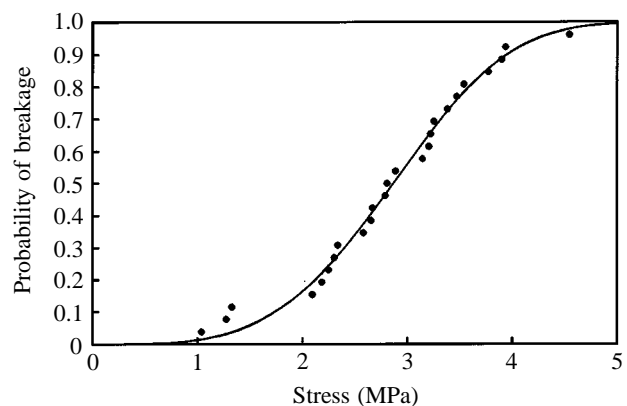


Fig. 6. The cumulative probability of stipe breakage as a function of tensile stress for *M. pyrifera*. The solid line is drawn from equation 21. See text for further details.

Table 1. Comparison of model results with field measurements

Measured force (N)	Predicted force (N)					
	Cycle 1	Fractional error	Cycle 2	Fractional error	Cycle 3	Fractional error
30.85	10.55	-1.925	10.07	-2.064	7.76	-2.974
23.64	24.28	0.026	23.70	0.002	24.37	0.030
15.00	17.53	0.144	18.53	0.191	20.92	0.283
14.52	16.61	0.126	17.66	0.177	19.24	0.245
10.66	15.04	0.291	13.01	0.181	13.43	0.206
10.42	12.65	0.176	13.02	0.199	13.53	0.230
8.07	16.11	0.499	13.80	0.415	14.11	0.428
6.32	10.13	0.377	9.29	0.320	9.46	0.332
6.02	7.28	0.172	7.27	0.172	9.35	0.357
5.83	11.90	0.510	10.25	0.431	10.99	0.470
5.10	9.85	0.482	9.82	0.481	9.84	0.482
4.93	10.85	0.546	8.81	0.441	9.47	0.480
4.67	10.80	0.568	8.08	0.422	9.01	0.482
3.93	10.66	0.630	10.43	0.622	10.44	0.622
2.47	10.04	0.754	8.71	0.716	8.92	0.723
1.91	10.97	0.826	10.63	0.820	10.65	0.821
1.38	9.79	0.859	9.67	0.820	9.67	0.856

The dimensionless added mass coefficient,  $C_a=3$ .

Fractional error determines the fit of the model to the field data (see text for further details).

The model performs best at predicting the larger forces encountered in the field. The mean fractional error for those trials in which the measured force exceeded 6 N (the nine largest measured forces) was  $-0.013$  to  $-0.096$ . Thus, in these cases, the model underestimates the force imposed on fronds in the field by an average of only 1.3–9.6%.

The nine largest forces measured in the field include a force of 30.85 N for which our model predicts a force of only 7.8–10.6 N (Table 1). This single, large underestimate on the part of the model affects the assessment of the model's fit to the field data. If this one value is excluded from the nine largest forces, the mean fractional error of the remaining eight is 0.21–0.26. The reason for the large disparity between prediction and observation in this single case is not known, although it is possibly due to the tangling of this frond with others on the same plant, a factor explored in greater depth in the Discussion.

Predictions of tension calculated for the second wave cycle after initiation of the model provide the best fit to the field data, overestimating the measured force by an average of 21% (Table 2; eight largest forces, the anomalous 30.85 N force excluded).

Varying the initial velocity of the point mass in the model had only a minor effect on the maximal predicted force. The calculation in which the point element had an initial velocity equal to the wave's orbital velocity yielded maximal forces that were on average 6.2% higher than those obtained when the initial velocity was zero. Given that the model has a general tendency to overestimate the force measured in the field

Table 2. The effect of the added mass coefficient,  $C_a$ , and wave cycle on the results of the model

$C_a$	Wave cycle	All forces		Selected large forces	
		Mean fractional error	S.E.M.	Mean fractional error	S.E.M.
1	1	0.414	0.082	0.438	0.086
1	2	0.457	0.073	0.495	0.052
1	3	0.478	0.068	0.518	0.048
2	1	0.392	0.096	0.406	0.052
2	2	0.409	0.092	0.444	0.043
2	3	0.436	0.086	0.476	0.038
3	1	0.298	0.147	0.226	0.051
3	2	0.258	0.152	0.207	0.040
3	3	0.240	0.206	0.264	0.040
4	1	-0.299	0.499	-0.238	0.442
4	2	-0.354	0.502	-0.289	0.408
4	3	-5.257	5.270	-0.178	0.282

The selected large forces are the eight largest measured forces, excluding the anomalous force of 30.85 N.

slightly (see above), the use of the stationary initial condition seems preferable.

## Discussion

### *An evaluation of the computational model*

At least two factors could contribute to the general tendency for our model to overestimate force. First, the model assumes that the vertical and horizontal velocities relative to the point element are an accurate measure of the velocities relative to fronds in the field. Because actual fronds are flexible and have finite size, this assumption cannot be precisely realized in nature. As the water's velocity changes direction, time must pass before real fronds move into a new alignment with the flow and again feel substantial drag. It thus seems likely that the drag calculations made as part of our model overestimate the drag acting on a real frond for at least part of the wave cycle.

Furthermore, our model assumes that all of a frond's mass is located at the center of drag. By making calculations for this point mass, we tacitly assume that, when the mass comes to the end of its tether, all of the mass is instantaneously affected by the tension in the stipe. In reality, the mass of a frond is widely distributed, and when the stipe becomes taut, the frond will be decelerated relatively gradually. The distribution of mass in the real frond may thus serve to reduce the rate of deceleration relative to that predicted by our model. However, without a more complex model in which distributed masses are taken into account, the importance of this effect cannot be evaluated.

Although improvements are certainly possible in our understanding of kelp dynamics, and more precise (and more complex) models can be written, we are pleased that a model

Table 3. Comparison of predicted fraction of stipes broken with field-measured kelp mortality

Depth (m)	1982/83		1986/87	
	Measured	Predicted	Measured	Predicted
13	0.66	0.128	0.94	0.173
16	0.47	0.016	0.69	0.262
19	0.13	0.001	0.65	0.015

as simple as ours comes as close as it does to explaining the hydrodynamic forces imposed on *M. pyrifera*.

#### Implications for kelp survivorship

The comparisons made above between model predictions and field data are based on short-term observations during relatively calm summer conditions. What does our model predict for stormier seas? To explore this question, we use the model to predict the forces imposed on *M. pyrifera* in southern California during the extreme storms associated with El Niño – Southern Oscillation (ENSO) events.

In the ENSO winters of 1982/83 and 1986/87, several large storms hit the kelp bed at Point Loma, California, a site where Seymour *et al.* (1989) conducted field censuses of *M. pyrifera*. The maximal significant wave height recorded during the winter by a buoy near the kelp bed was 4.8 m in 1982/83 and the wave period was 18 s. The corresponding data for 1986/87 were 6.7 m and 13 s. If we assume that these energetic sea states were each present for a period of 8 h (the interval between measurements of significant wave height), the maximal wave heights encountered by the bed were 9.0 m in 1982/83 and 12.6 m in 1986/87 (see equation 13).

We calculate the tension that would be imposed by these wave heights during the second wave cycle on an average frond at each of the three depths monitored by Seymour *et al.* (1989) (13, 16 and 19 m). Characteristics of the average frond are obtained from measurements taken on 16 fronds collected at Cabrillo Point. For these fronds (ranging in length from 11.75 to 24.80 m), there was no significant correlation between frond length and either buoyancy or the minimal cross-sectional area of the stipe. The average buoyancy was 2.49 N and the average stipe cross-sectional area was  $4.1 \times 10^{-5} \text{ m}^2$ . These values were used for fronds at all depths. Frond maximal projected area,  $A$ , was correlated with length in our sample. Areas ( $\text{m}^2$ ) were regressed against frond length,  $l_f$  (in m) in an allometric relationship using untransformed data and a simplex algorithm:

$$A = 0.297 l_f^{0.955} \quad (23)$$

This relationship is statistically significant ( $P < 0.002$ ) and explains 38% of the variance in frond area. Frond mass was calculated from frond area as described previously.

In our calculations of force as a function of wave height, the average frond is given an overall length equal to the ocean depth. A corresponding buoyancy, frond area and wet mass were obtained from the relationships described above. It was assumed that the effective length of the stipe (the stipe length

at the center of drag) was equal to 0.8 times the overall length of the stipe (a typical value observed in the field data).

Given the extreme wave height of 9 m for the 1982/83 calculation and 12.6 m for the 1986/87 calculation, it is necessary to consider the possibility that waves have broken by the time they reach the depth in question. If the slope of the seafloor is gentle (as it is at Point Loma), it is generally accepted that waves break if their height exceeds 78% of the water's depth (US Army Corps of Engineers, 1984; Denny, 1988; Seymour *et al.* 1989). Thus, waves with a height in excess of 10.1 m will have broken by the time they reach a depth of 13 m, and waves with a height in excess of 12.5 m will have broken when they arrive at a depth of 16 m. Therefore, the maximal wave height predicted for the 1986/87 storm (12.6 m) is likely to be higher than that which would actually occur at the 13 m and 16 m sites. In these cases, the maximal wave height is set equal to the theoretical breaking height. The subject of wave breaking is treated in more depth below.

The probability of stipe breakage predicted by our model is relatively small, ranging from 0.1 to 26.2% (Table 3). Note that, in making these predictions, we have not attempted to correct our model for its tendency to overestimate forces imposed on kelps. Thus, the predicted values cited here may actually overestimate the damage that can be expected when hydrodynamic forces interact with individual fronds.

The percentage of stipes predicted to break in storms (0.1–26.2%) is substantially smaller than the percentage of kelp mortality measured in the field by Seymour *et al.* (1989) (13–94%, Table 3), a disparity that may be even larger than these numbers suggest. In their survey of kelp mortality, Seymour *et al.* (1989) counted a plant as dead only if the entire plant (holdfast included) was absent from its previously marked spot on the substratum. By this definition, breakage of even a substantial fraction of the fronds on one holdfast (an event many holdfasts survive) would not be counted as mortality.

It is clear that the high rates of mortality observed by Seymour *et al.* (1989) cannot be accounted for directly on the basis of stipe breakage as predicted by our model. In this respect, the results of our model are consistent with the observation of Seymour *et al.* (1989) that kelp mortality in southern California is due primarily to dislodgment of the holdfast by the combined action of sub-breaking forces acting on several stipes.

In summary, our model predicts that individual stipes are well designed to resist the hydrodynamic forces imposed by even very large waves. Complications intrinsic to the combined interaction of many stipes may, however, lead to higher rates of mortality than predicted for individual stipes. For example, many fronds are anchored by a single holdfast. If two or more fronds become entangled, one stipe may have to resist the additional drag of its neighbors and may therefore experience an increased risk of breakage. This effect may be most important in large plants which have more fronds and are thus more likely to become entangled (Seymour *et al.* 1989). Large rafts of tangled *M. pyrifera* plants have been observed

after storms (Dayton *et al.* 1984; Seymour *et al.* 1989), and Dayton *et al.* (1984) propose that entanglements with drifting rafts of tangled fronds are a substantial contributor to holdfast dislodgment in the Point Loma kelp forest.

The possibility that the entanglements of stipes can contribute to breakage suggests that kelp species with solitary fronds may have a relatively greater chance of surviving wave forces. For instance, the giant kelp *N. luetkeana* has only one stipe per holdfast, in contrast to *M. pyrifera* in which tens of stipes may grow from a single holdfast. This scenario would suggest that owing to a lowered rate of entanglement, *N. luetkeana* could survive greater wave exposure than *M. pyrifera*. Indeed, in central California, *N. luetkeana* is typically found on shores that are more exposed than those inhabited by *M. pyrifera*, and the difference has been attributed at least in part to the inability of *M. pyrifera* to persist in the face of more extreme hydrodynamic forces (Dayton *et al.* 1984).

In addition, wave breaking may cause forces greater than those our model predicts. As waves move into shallower water, their height tends to increase and their wavelength decreases (Denny, 1988). As a result, waves become steeper, and at a critical height they become unstable and break. The critical breaking height can vary from 0.78 times the local water depth to approximately 1.4 times the depth, depending on the wave period and the slope of the seafloor (US Army Corps of Engineers, 1984; Denny, 1988). When a wave breaks, the water at its crest moves at a velocity equal to that of the waveform (forming the 'roller' characteristic of broken waves), and this velocity is often substantially faster than the orbital velocity of water below the surface. If waves break prior to their interaction with kelps, it is possible that the surface blades of a frond may be subjected to the increased drag and accelerational forces caused by flow in the roller. Seymour *et al.* (1989) speculate that wave breaking may thus elevate the rate of stipe breakage and dislodgment in *M. pyrifera*, but note that the effect will be difficult to model. Owing to the presence of entrained air, the density of water in the roller of a broken wave is low relative to that of water below the surface. As a consequence, it is unclear how much of a surface blade would actually extend into the area of rapid flow in a roller, which makes prediction of the effects of wave breaking problematic.

Other physical factors may also contribute to stipe breakage. These factors include the impact of rocks propelled by hydrodynamic forces (which may injure stipes and holdfasts) and secondary effects of storms, such as wind-driven surface currents (see review by Seymour *et al.* 1989). Changes in water temperature (e.g. those associated ENSO events) may also affect the health (and thereby the strength) of kelps (Dayton and Tegner, 1984; Tegner and Dayton, 1987).

In addition to these physical factors, there are several biological factors that may affect kelp breakage. For example, it is possible that as a plant ages the strength of its stipes changes (Johnson and Koehl, 1994), and the age structure of a kelp bed may thus be a factor in the probability of breakage (Seymour *et al.* 1989).

Kelps can also respond to their physical environment by

changing their morphology. For example, Gerard (1987) found that when *Laminaria saccharina* was subjected to tensile forces that mimicked drag, it grew with a more streamlined shape. Johnson and Koehl (1994) found differences in morphology among populations of *N. luetkeana* that tended to maintain a constant risk of breakage. Because of the plasticity of kelp morphology, it may be necessary to adjust the predictions made on the basis of plants sampled at one site when applying these data to different sites.

And lastly, herbivory by invertebrates (such as sea urchins) may contribute to kelp breakage by wounding stipes, thereby decreasing their tensile strength. Grazing on stipes has been suggested to contribute to the mortality of *N. luetkeana* (Koehl and Wainwright, 1977).

The technical help and field assistance of J. Watanabe was invaluable and it was due to his assistance that we were able to obtain wave data at Point Joe. In addition, we appreciate the extensive field assistance, advice and companionship of E. C. Bell. Drag data collection was carried out with the aid of W. Hoese, S. Distefano, S. Worcester and D. Olson. We would also like to thank those people who assisted by SCUBA diving: S. Alin, D. Anderson, G. Bernardi, J. Coyer, N. Crane, A. Cronin, H. Farrington, B. Heywood, G. Leonard, G. Kraemer, C. Lichtendahl, D. Nelson, J. Shaw, G. Suba, A. Welsch and S. Wooster. This study was supported by NSF grant OCE 87-11688 and OCE 91-15688 to M. Denny.

## References

- BATCHELOR, G. K. (1967). *An Introduction to Fluid Mechanics*. Cambridge: Cambridge University Press.
- BELL, E. C. (1992). Consequences of morphological variation in an intertidal macroalgae: Physical constraints on growth and survival of *Mastocarpus papillatus* Kützting. PhD dissertation, Stanford University, Stanford, California.
- BELL, E. C. AND DENNY, M. W. (1994). Quantifying 'wave exposure': a simple device for recording maximum velocity and results of its use at several field sites. *J. exp. mar. Biol. Ecol.* **181**, 9–29.
- CACECI, M. S. AND CACHERIS, W. P. (1984). Fitting curves to data: the Simplex algorithm is the answer. *BYTE* **9**, 340–362.
- CARRINGTON, E. (1990). Drag and dislodgment of an intertidal macroalga: consequences of morphological variation in *Mastocarpus papillatus* Kützting. *J. exp. mar. Biol. Ecol.* **139**, 185–200.
- DAHLQUIST, G. AND BJÖRK, Å. (1974). *Numerical Methods*. Englewood Cliffs, NJ: Prentice-Hall, Inc.
- DAYTON, P. K., CURRIE, V., GERRODETTE, T., KELLER, B. D., ROSENTHAL, R. AND VEN TRESKA, D. (1984). Patch dynamics and stability of some California kelp communities. *Ecol. Monogr.* **54**, 253–289.
- DAYTON, P. K. AND TEGNER, M. J. (1984). Catastrophic storms, *El Niño* and patch stability in a Southern California kelp community. *Science* **224**, 283–285.
- DENNY, M. W. (1987). Life in the maelstrom: The biomechanics of wave-swept rocky shores. *Trends Ecol. Evol.* **2**, 61–66.
- DENNY, M. W. (1988). *Biology and the Mechanics of the Wave-Swept Environment*. Princeton, NJ: Princeton University Press.
- DENNY, M. W. (1989). A limpet shell shape that reduces drag:

- Laboratory demonstration of a hydrodynamic mechanism and an exploration of its effectiveness in nature. *Can. J. Zool.* **67**, 2098–2106.
- DENNY, M. W. (1993). Disturbance, natural selection and the prediction of maximal wave-induced forces. *Contemp. Math.* **141**, 65–90.
- DENNY, M. (1995). Predicting physical disturbance: Mechanistic approaches to the study of survivorship on wave-swept shores. *Ecol. Monogr.* **65**, 371–418.
- DENNY, M. W., DANIEL, T. L. AND KOEHL, M. A. R. (1985). Mechanical limits to size in wave-swept organisms. *Ecol. Monogr.* **55**, 69–102.
- ECKART, C. (1952). The propagation of waves from deep to shallow water. In *Gravity Waves*, National Bureau of Standards, Circular No. **521**, 165–173.
- FRIEDLAND, M. T. AND DENNY, M. W. (1995). Surviving hydrodynamic forces in a wave-swept environment: Consequences of morphology in the feather boa kelp, *Egregia menziesii* (Turner). *J. exp. mar. Biol. Ecol.* **190**, 109–133.
- GAYLORD, B., BLANCHETTE, C. AND DENNY, M. W. (1994). Mechanical consequences of size in wave-swept algae. *Ecol. Monogr.* **64**, 287–313.
- GERARD, V. A. (1987). Hydrodynamic streamlining of *Laminaria saccharina* Lamour in response to mechanical stress. *J. exp. mar. Biol. Ecol.* **107**, 237–244.
- GUMBEL, E. J. (1958). *Statistics of Extremes*. New York: Columbia University Press.
- JACKSON, G. A. AND WINANT, C. D. (1983). Effect of a kelp forest on coastal currents. *Continental Shelf Res.* **2**, 75–80.
- JOHNSON, A. S. AND KOEHL, M. A. R. (1994). Maintenance of dynamic strain similarity and environmental stress factor in different flow habitats: thallus allometry and material properties of giant kelp. *J. exp. Biol.* **195**, 381–410.
- KINSMAN, B. (1965). *Wind Waves*. Englewood Cliffs, NJ: Prentice-Hall.
- KOEHL, M. A. R. (1984). How do benthic organisms withstand moving water? *Am. Zool.* **24**, 57–70.
- KOEHL, M. A. R. (1986). Seaweeds in moving water: Form and mechanical function. In *On the Economy of Plant Form and Function* (ed. T. J. Givnish), pp. 603–634. Cambridge: Cambridge University Press.
- KOEHL, M. A. R. AND WAINWRIGHT, S. A. (1977). Mechanical design of a giant kelp. *Limnol. Oceanogr.* **22**, 1067–1071.
- LONGUET-HIGGINS, M. S. (1952). On the statistical distribution of the heights of sea waves. *J. mar. Res.* **11**, 245–266.
- LONGUET-HIGGINS, M. S. (1980). On the distribution of the heights of sea waves: some effects of nonlinearity and finite bandwidth. *J. Geophys. Res.* **85**, 1519–1523.
- NEUSHUL, M., CLARKE, W. D. AND BROWN, D. W. (1967). Subtidal plant and animal communities of the southern California islands. *Proceedings of the Symposium on the Biology of California Islands* (ed. R. N. Philbrick), pp. 37–55. Santa Barbara, California.
- NORTH, W. J. (1971). (ed.) The biology of giant kelp beds (*Macrocystis*) in California. *Nova Hedwigia* **32**, 1–97.
- SARPKAYA, T. AND ISAACSON, M. (1981). *Mechanics of Wave Forces on Offshore Structures*. New York: Van Nostrand Reinhold.
- SEYMOUR, R. J., TEGNER, M. J., DAYTON, P. K. AND PARNELL, P. E. (1989). Storm wave induced mortality of giant kelp, *Macrocystis pyrifera*, in southern California. *Est. Coast. Shelf Sci.* **28**, 277–292.
- TEGNER, M. J. AND DAYTON, P. K. (1987). *El Niño* effects on southern California kelp forest communities. *Adv. Ecol. Res.* **17**, 243–279.
- US ARMY CORPS OF ENGINEERS (1984). *Shore Protection Manual*, 4th edn. Washington, DC: US Government Printing Office.
- VOGEL, S. (1984). Drag and flexibility in sessile organisms. *Am. Zool.* **24**, 37–44.
- VOGEL, S. (1989). Drag and reconfiguration of broad leaves in high winds. *J. exp. Bot.* **40**, 941–948.
- VOGEL, S. (1994). *Life in Moving Fluids*, 2nd edn. Princeton, NJ: Princeton University Press.